Bulletin of the Seismological Society of America, Vol. 102, No. 1, pp. 436–444, February 2012, doi: 10.1785/0120110025

Short Note

Crustal-Scale Weak Zone along a Collisional Suture Revealed by Spatial Variations in Velocity Structures and Seismicity

by Kwang-Hee Kim, Kou-Cheng Chen, Jer-Ming Chiu, and Horng-Yuan Yen

Abstract High-quality first-arrival data collected with a high-density temporary seismic array and regional seismic network were used to construct a *P*-wave velocity model and identify the precise location of earthquakes in the active collision zone of southeastern Taiwan. A crustal-scale weak zone, defined by high seismicity, is characterized by a steeply east-dipping lower-velocity anomaly and represents a boundary between an uplifted upper-mantle and the Luzon volcanic arc. The main features of the weak zone, with its associated low-velocity zone and seismicity pattern, vary significantly along the collisional boundary of southeastern Taiwan. Along the weak zone, unlithified sediments or highly fractured materials are compacted as the Philippine Sea plate moves toward the Eurasian plate. In areas of more advanced collision, soft material is more compacted and can therefore store significantly greater amounts of strain energy. This energy is released through episodic earthquakes.

Introduction

Taiwan is one of the most seismically active regions on Earth. The tectonic framework of the region is dominated by a collision zone sandwiched between two subduction systems: the Ryukyu trench to the northeast and the Manila trench to the south. Topographic trend of Taiwan and its structural and lithological units are aligned with the north-northeast trending collision system (Teng, 1990). At the center of the region is the Longitudinal Valley (LV), a narrow, 160-km long, topographic feature that is generally regarded as the boundary between the Eurasian and the Philippine Sea plates (Fig. 1; Ho, 1988). Large topographic relief, concentration of high seismicity, and evidence from geodetic measurement have revealed that two active fault systems run parallel with each other along the entire length of the LV, although their surface expressions are obscured by thick fluvial deposits. The east- and west-flanking faults of the LV are the east-dipping Longitudinal Valley fault (LVF) and the near-vertical Central Range fault, respectively (Kim *et al.*, 2006; Wu *et al.*, 2006).

The Coastal Range (CR) is the result of the accretion of the Luzon arc-forearc to the exhumed metamorphic basement of eastern Taiwan during arc–continent collision over the last two million years (Chai, 1972; Huang *et al.*, 2008). Stratigraphic and geochemical studies have shown that the CR is composed of three accreted Miocene–Pliocene volcanic islands (Yuehmei, Chimei, and Chengkungao), three Plio-Pleistocene remnant forearc basins (Shuilien, Loho, and Taiyuan), two intra-arc basins (Chingpu and Chengkung), and the Pliocene Lichi mélange. Accreted volcanic arcs are composed of andesite, agglomerates, and tuff. Basins are filled with turbidites derived from the accretionary prism. The Lichi mélange includes chaotic mudstones intermixed with exotic blocks of ophiolitic, sedimentary, and andesitic rocks (Huang *et al.*, 1995; Chang *et al.*, 2001; Huang *et al.*, 2008).

Collision is understood to be the most pronounced in the northern LV and CR, owing to the obliquity of plate convergence. This implies that incipient collision will develop at the southern end of the LV, but the exact location and detailed structure of such a phenomenon is not known. This study examined the crustal-scale structure of deformation in this active collision zone using a high-resolution V_P model and relocated seismicity. Important features, such as lateral variations in subsurface structure and seismicity patterns, were found in the transition zone between areas of initial and advanced collision.

Data and Methods

Two sets of high-quality earthquake data recorded by an island-wide seismic network and a local high-density temporary seismic network were used to define a 3D *P*-wave velocity model. The Central Weather Bureau Seismic Network (CWBSN), the major earthquake-monitoring network in Taiwan since 1991, consists of 71 stations equipped with three-component S13 seismometers. Twenty-three CWBSN stations are in the study area. Data from the CWBSN earthquake catalog from January 1991 to September 2009 were

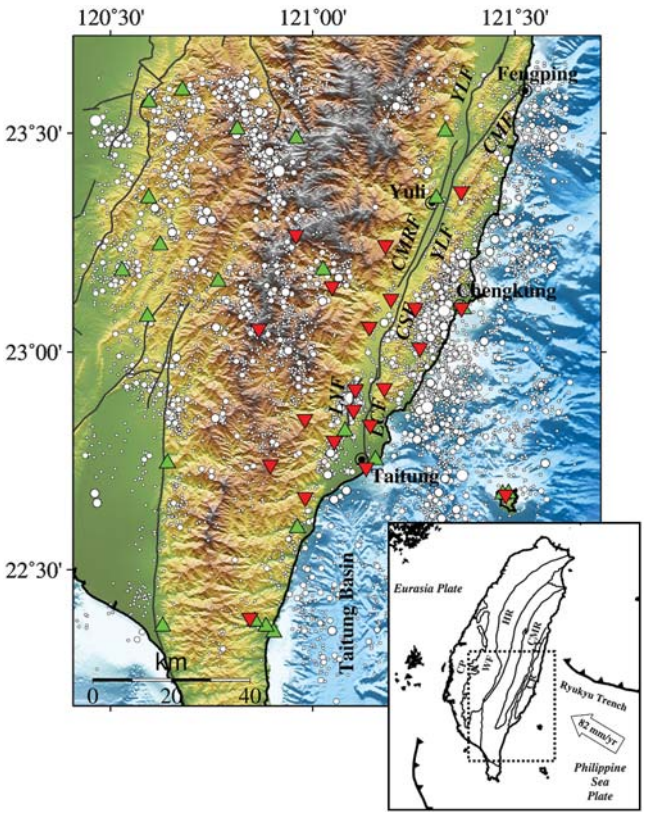

Figure 1. Topographic and bathymetric map of the collision zone in southeastern Taiwan. Longitudinal Valley (LV) is distinguished by a narrow and long topographic-low feature. It is bounded by two active fault systems running parallel to each other along the entire length of LV. Western and eastern boundary fault of LV is the Central Range fault system (CMRF, Central Mountain Range fault; LYF, Luveh fault) and the Coastal Range fault system (YLF, Yuli fault; CSF, Chishang fault; LCF, Lichi fault), respectively. An active fault (CMF, Chimei fault) is also observed in the northern Coastal Range. General geological divisions in Taiwan are presented in the index map (CP, Coastal plain; WF, Western foothills; HR, Hsueshan Range; CMR, Central Mountain Range; LV, Longitudinal Valley; CR, Coastal Range). Dotted box in the index map marks the area of the larger map. White circles are relocated earthquake epicenters with radii scaled to magnitude. PANDAII and CWBSN seismic stations used in the tomographic inversion are presented in red and green triangles, respectively.

collected and analyzed. A second data set from a high-density temporary earthquake-monitoring array, the Portable Array for Numerical Data Acquisition II (PANDA II), in southeastern Taiwan was collected by the Institute of Earth Sciences, Academia Sinica, and the Center for Earthquake Research and Information of the University of Memphis, from September 1995 to July 1996 (K. C. Chen, 1995). PANDA II consisted of 23 three-component short-period seismic stations, of which two were located outside the study area. High-quality earthquake data from 21 stations located near the center of the study area were used to formulate a high-resolution *P*-wave velocity model.

Selection criteria for earthquake data were established to ensure the best possible ray path coverage of the study area using the available data sets. Events with more than six high-quality *P* arrivals (i.e., with arrival time uncertainty less than 0.5 s) were selected. Event-station pairs with an epicentral distance greater than 120 km were excluded for a better approximation of a flat Earth (Snoke *et al.*, 2001). The selected earthquakes occurred at depths shallower than 65 km. More than 18,000 earthquakes satisfied these initial criteria. The study area was then divided into $4 \times 4 \times 2$-km^3 cells, and from the seismic events that took place in each cell, the two events recorded by the most stations were selected. The final data subset selected for the 3D tomographic inversion incorporated 78,403 first-arrival-time readings from 9456 earthquakes recorded by 44 seismic stations.

The 3D *P*-wave velocity model was determined using a software package initially developed by Benz *et al.* (1996). The package calculates first-arrival times using a finite-difference solution of the Eikonal equation, which was designed to handle large velocity variations (Vidale, 1988; Podvin *et al.*, 1991). This method has been successfully applied to data from complex tectonic environments with large velocity contrasts (Shen, 1999; Kim *et al.*, 2005; Mandal *et al.*, 2006; Kim *et al.*, 2010). This software package is therefore considered suitable for the establishment of a subsurface velocity model in the study area, which is characterized by a very complex structure.

Earthquakes recorded by the CWBSN and PANDA II were initially located using a 1D horizontally layered velocity model, which is commonly a source of significant location error, especially for structurally complex regions. Earthquakes are relocated during tomographic inversions using the resultant 3D velocity model. Lengthy travel-time calculations are one of the major hindrances when using a 3D velocity model in earthquake locations. Chen *et al.* (2006) developed an efficient and stable algorithm to handle travel-time calculations across 3D velocity models for a single earthquake location. The algorithm stores 3D travel times on file to corresponding grid points. During single event locations, travel times from the trial hypocenter to the recording stations can be determined by linear interpolations from those at the adjacent eight grid points. This algorithm does not use lengthy travel-time calculations. In this study, all of the events in the earthquake catalog were relocated after the determination of the 3D velocity model to take advantage of the abundant seismicity available for tectonic interpretation.

Results and Discussion

The study area in southeastern Taiwan covers an area of 136 km × 168 km, where active collision is ongoing. The vertical thickness of the velocity model was 74 km, which included 4 km above and 70 km below sea level. The study area was parameterized for the velocity inversion using a uniform grid with a $4 \times 4 \times 2$ km^3 cell size. A smaller cell size ($1 \times 1 \times 1$ km^3) was used for a more precise estimation of the shortest travel times between sources and receivers. Optimum damping and smoothing values were selected

following the method of Eberhart-Phillips (1986). A horizontally layered 1D velocity model proposed by Y. L. Chen (1995) was used as an initial velocity model for the inversion. Finally, a 3D *P*-wave velocity model was obtained after nine iterations. The root-mean-square (rms) residual of arrival times decreased from 0.69 to 0.26, which is equivalent to 62.2% of an rms residual reduction.

Checkerboard resolution tests (CRTs) were used to examine the resolution power of subsurface structures for the given station-event configurations (Zhao *et al.*, 1992). The CRT results showed checkerboard perturbation patterns at depths from 4 to 40 km (Fig. 2). Regions at the periphery of the study area cannot be properly resolved primarily because of insufficient ray coverage. Therefore, our interpretation of results focus on areas with sufficient CRT resolution.

For areas with adequate ray coverage, similar inversion results were obtained when slightly different initial 1D models were used. The dominant features of the final models do not appear to depend on the initial input details. The resultant velocity model obtained from the inversion is considered robust, although some structural features may be poorly constrained at the periphery of the model where ray coverage is inadequate or the station spacing is relatively large. In general, the highest resolution of the velocity structure is observed in the central part of the study area where high-quality data are available from the high-density temporary array (PANDA II) as shown in the checkerboard test (Fig. 2).

Initial and relocated earthquake locations are presented in Figures 3 and 4 in plane and cross-sectional views, respectively. As a rule, the quality of an earthquake's location is less precisely known when the earthquake occurs outside the monitoring seismic network. Chiu *et al.* (1997) and Chen *et al.* (2006), however, demonstrated that an earthquake occurring outside a seismic network can be located reasonably well using reliable velocity models. As demonstrated by the checkerboard resolution test in Figure 2, the 3D velocity

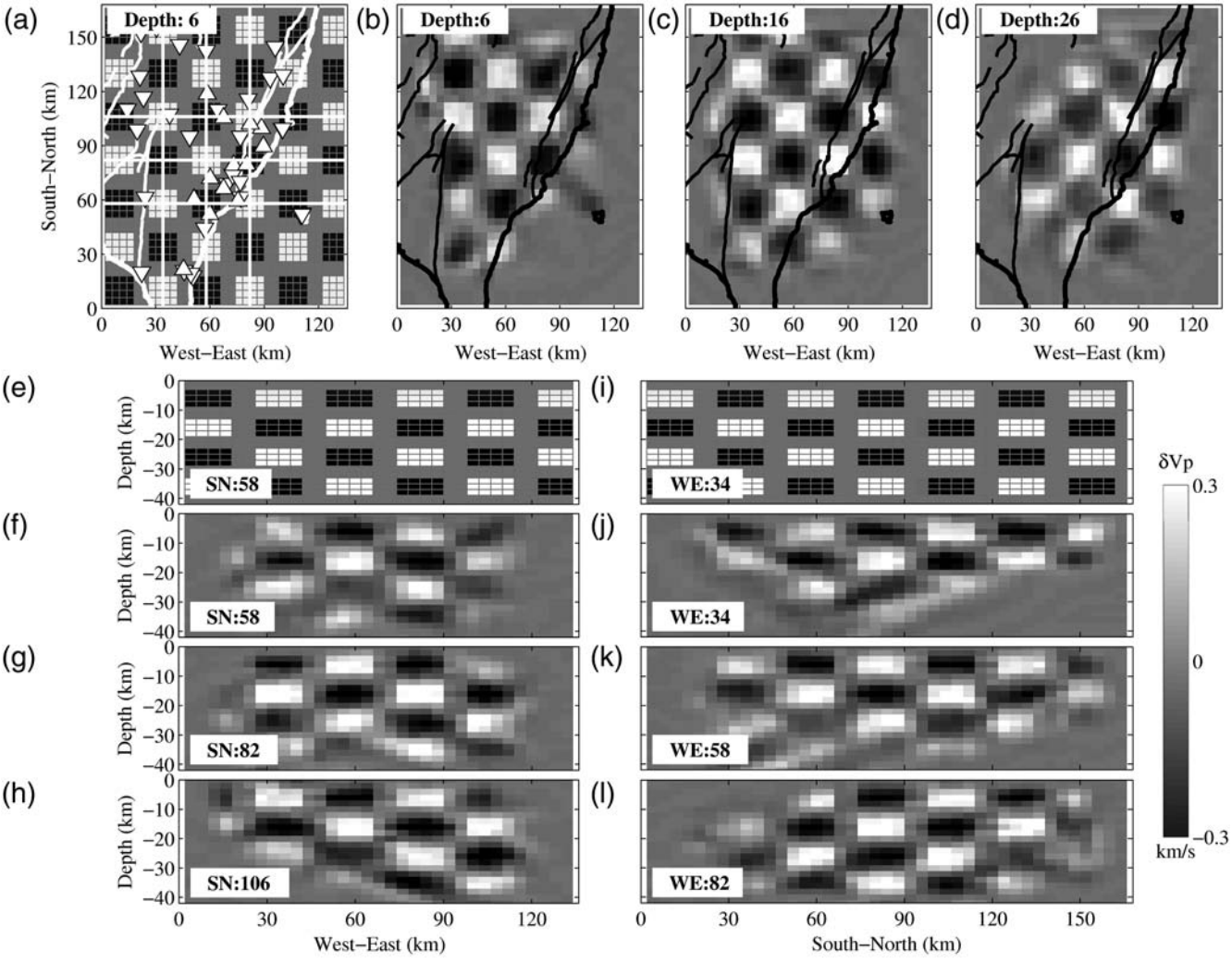

Figure 2. Results of a checkerboard resolution test. (a) $+/-5\%$ of velocity perturbation applied to the initial velocity model. Each checkerboard block is $4 \times 4 \times 3$ cells, which corresponds to a volume of $16 \times 16 \times 6$ km^3. (b)–(d) Map view of the restored checkerboard velocity model at depths of 6 km, 16 km, and 26 km. (e)–(l) Cross-sectional views of the initial and restored checkerboard velocity model at select locations shown in the lower left.

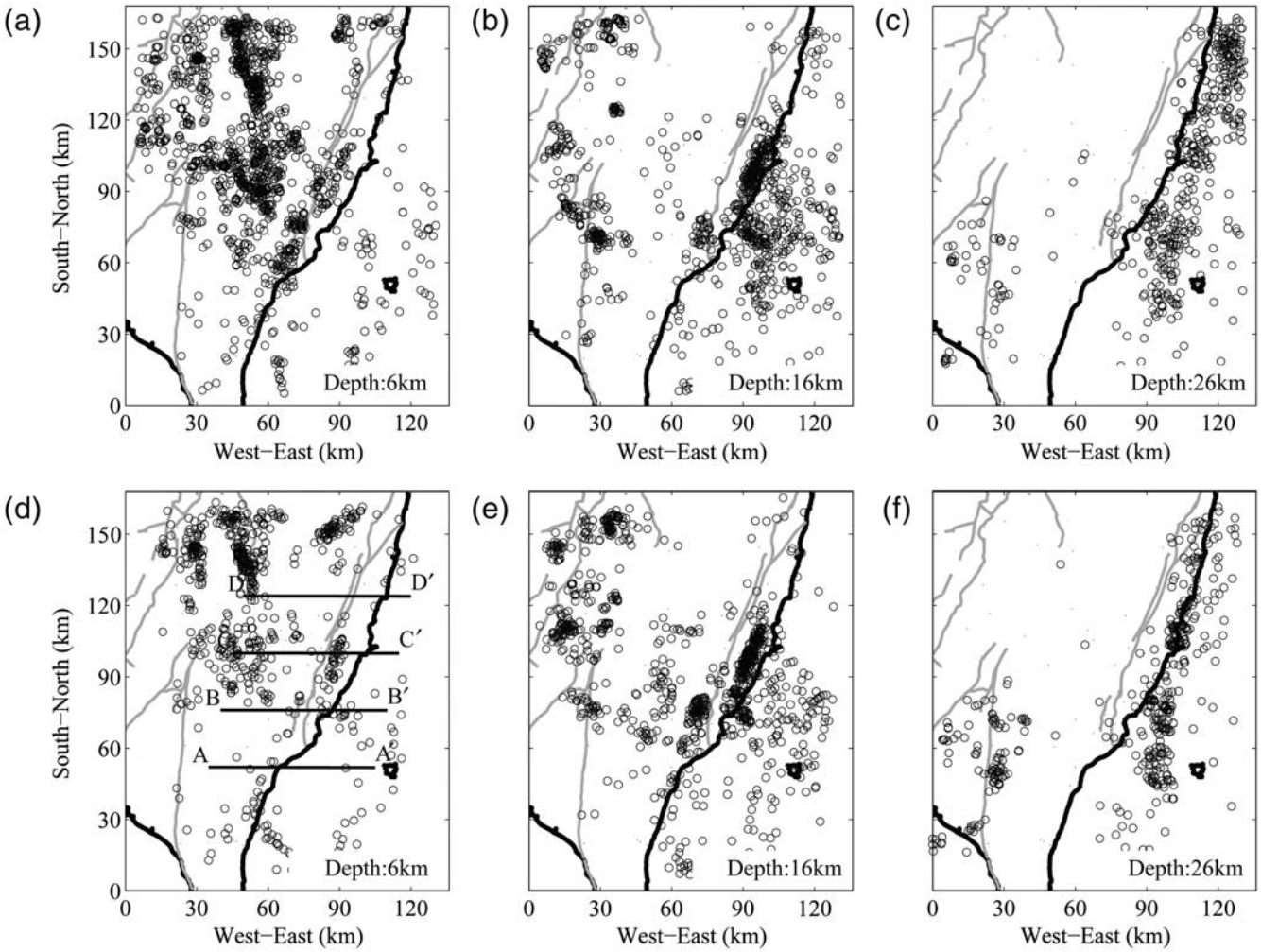

Figure 3. Plane views of earthquake epicenters of >3 magnitude. Data shown are from 1991 to 2009. (a)–(c) Earthquake locations determined and reported by CWBSN. (d)–(f) Relocated earthquake epicenters using the 3D velocity model in the study. Focal depths of the presented earthquakes are within 2 km from the depth shown in the lower right corner. Major active faults are shown by gray solid lines (see Fig. 1). Locations of profiles for cross-sectional views of seismicity in Figure 4 are shown in (d).

model used in this study is clearly representative of the lateral and vertical velocity variations in the offshore areas. The rms residual of arrival times for all earthquakes is reduced from 0.84 s to 0.37 s after relocation using the 3D velocity model. Initial rms residuals of onshore and offshore earthquakes are 0.79 s and 1.12 s, respectively. The difference in rms residuals partially supports the conventional idea of the geometry of a seismic network and its earthquake location quality. After relocation using the 3D velocity model, rms residuals of onshore and offshore earthquakes are reduced to 0.37 s and 0.38 s, respectively. Assuming the 3D velocity model is reliable, we observe that both onshore and offshore earthquakes are comparably well determined. Also, earthquakes are more tightly clustered after relocation, as both plane and cross-sectional views of earthquake hypocenters reveal.

Three-dimensional *P*-wave tomographic inversion results are presented in Figure 5. Large lateral velocity variations are apparent in the horizontal thin-sliced view of the 3D *P*-wave velocity model at 6-km depth (Fig. 5a). Results of the CRTs between 4- and 10-km depth revealed that the subsurface blocks were well-defined by seismic waves and that lateral structural variations were also successfully recovered (Fig. 2). This enabled shallow structures to be compared and correlated with surface geology. For example, a region of negative velocity anomaly beneath the western foothills in the northwestern part of the study area was associated with an area of relatively thick sedimentary deposits (Kim *et al.*, 2005; Wu *et al.*, 2007). Beneath the Central Range, a shallow high-velocity anomaly was associated with surface exposures of highly metamorphosed rocks. A strong, negative velocity anomaly farther to the east beneath the LV and CR may correspond to a region of thick, unconsolidated fluvial sediment in the LV, or poorly lithified sedimentary blocks in the CR. In general, an excellent correlation is observed between surface geology and the upper 6-km *P*-wave velocity model.

The overall distribution of *P*-wave velocity at 16-km depth (Fig. 5b) is quite different from that at 6-km depth. Lower *P*-wave velocities dominate at this depth under the

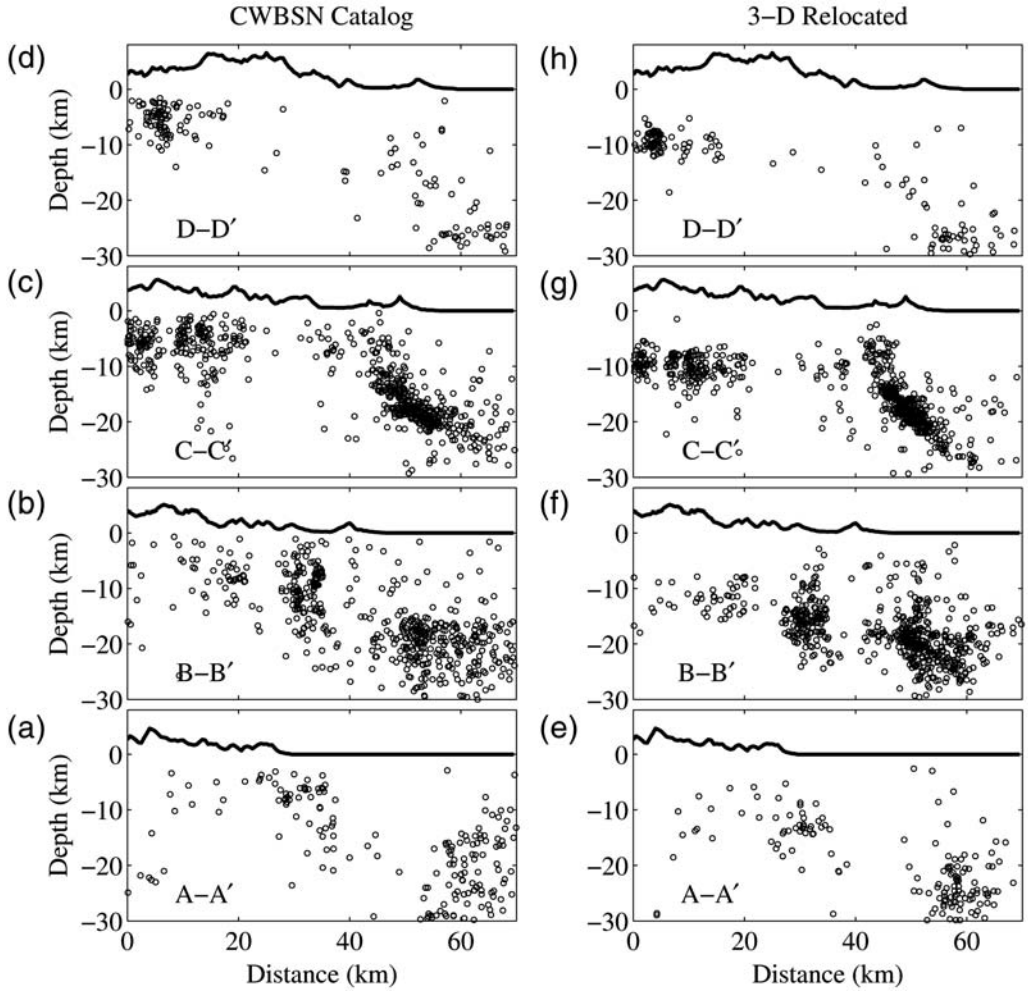

Figure 4. Sectional views of (a)–(d) the CWBSN earthquake catalog and (e)–(h) relocated earthquake hypocenters along profiles shown in Figure 3(d). Data shown are from 1991 to 2009 for earthquakes with a magnitude > 3. Earthquakes show tighter clustered in (e)–(h) than in (a)–(d). Also, note earthquake hypocenters along B–B′ present rather wide seismogenic zones at depths deeper than 15 km. In a northern profile along the C–C′, earthquake hypocenters form a tightly clustered planar seismogenic zone.

Central Range. A long and narrow zone of positive velocity anomaly is apparent beneath the LV and offshore areas to the south. A linear low-velocity feature is present to the east and lies subparallel to the adjacent high-velocity anomaly (marked by dotted lines in Fig. 5b). Relatively low *P*-wave velocities in the southern CR were related to the strong low-velocity anomaly observed at the 6-km depth slice of the velocity model, which have been emplaced by the accretion of remnant forearc and intra-arc basins and the Lichi mélange in the last 2 m.y. (Chai, 1972; Huang *et al.*, 2008). Another low-velocity anomaly in the mid-CR is apparent (marked by dotted lines in Fig. 5b). It is thought to represent a previously accreted forearc basin, which has been observed at the surface in the CR (Huang *et al.*, 1995; Huang *et al.*, 2008). Farther to the east, the tomographic image presents a high-velocity feature offshore of the CR, which represents the detached Luzon volcanic arc. In general, no clear correlation exists between the thin-sliced views of the velocity perturbations at 6- and 16-km depths.

At a depth of 26 km (Fig. 5c), the low-velocity perturbation beneath the Central Range is still apparent. The high-velocity zone, trending north-northeast beneath the CR, is continuous with the high-velocity anomaly documented at 16-km depth, although the former has a limited eastward displacement. The features present at a 16-km depth appear to continue down to a 26-km depth with diminishing amplitude.

Cross-sectional views of the *P*-wave velocity model are shown in Figure 6a–d. The percent perturbation of *P*-wave velocity anomaly to the background velocity ($\delta V_P/V_P$) is also shown for easier comparison in Figure 6e–h. Gray dots indicate earthquake hypocenters of magnitude > 3 that occurred between 1991 and 2009. At depths shallower than 8 km, *P*-wave velocity beneath the Central Range was higher than the background velocity, which is attributable to the highly metamorphosed rocks visible at the surface of the region. In contrast, low-velocity anomalies are distributed in large areas beneath the Central Range below a 14-km depth.

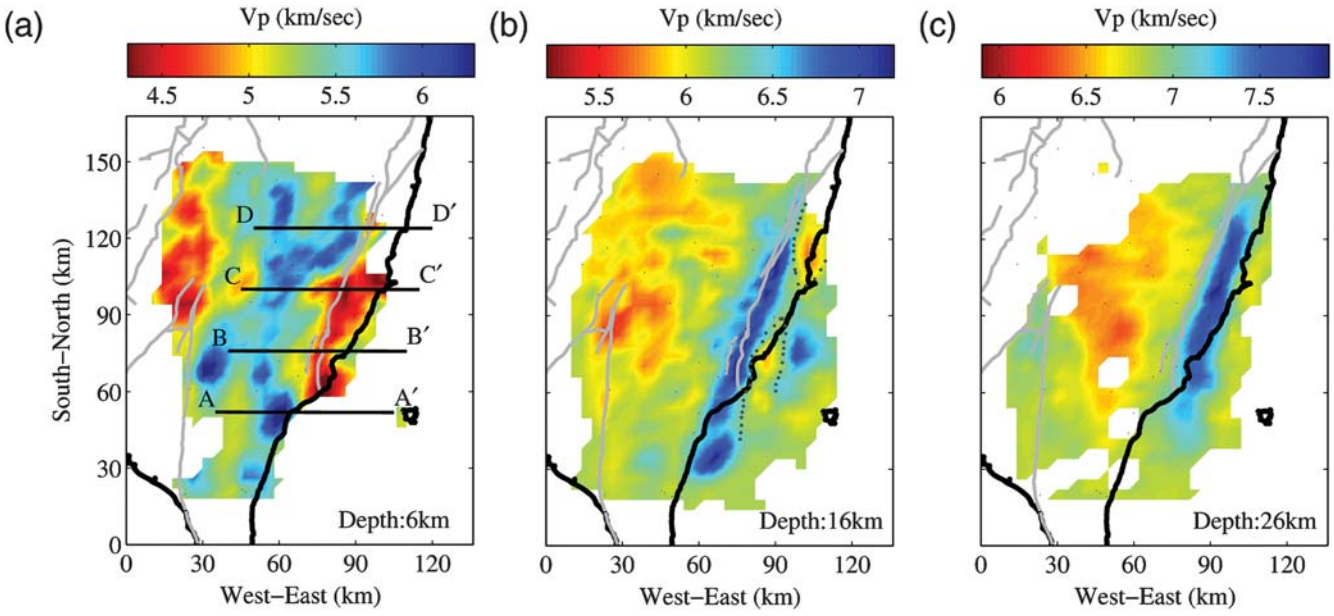

Figure 5. Plane view of the recovered velocity model at selected depths (given in lower right corners). Low-velocity anomalies discussed in the text are outlined by dotted lines. Major active faults are marked by gray lines. Locations of profiles for cross-sectional views of *P*-wave velocity anomaly (in Fig. 6) are shown in (a).

A region of low-velocity is dominant at shallow depths (< 10 km) beneath the LV and CR along profiles B–B′ and C–C′ (Fig. 6b,c,f,g) and are attributable to thick fluvial sediments in the LV. At depths of 14 km and deeper, however, a region of high-velocity anomaly is present beneath the LV along all profiles (Fig. 6). Previous studies on seismic tomography and detailed analysis of *Pn* wave travel times have supported the theory that this region of high-velocity material is the result of a relatively thin crust caused by an elevated oceanic upper-mantle due to plate collision and subsequent exhumation (Lin *et al.*, 1998; Kim *et al.*, 2005; Kim *et al.*, 2006; Liang *et al.*, 2007).

Beneath the eastern offshore area in profile B–B′ (Fig. 6b,f), a region of high-velocity anomaly at shallow depths (< 20 km) was correlated with the detached northern Luzon arc. This region of high-velocity anomaly appears to be independent of the high-velocity anomaly at depths below 14 km beneath the LV and CR. The two high-velocity regions/zones are separated by a thin, east-dipping, low-velocity zone that extends from the surface to a depth of at least 15 km. This anomalous zone coincides spatially not only with a lithologic boundary between the two colliding plates but also with a high seismicity zone extending to depths greater than 15 km. The seismicity in this zone spans a wide area that narrows northward to profile C–C′, where it forms a narrow band of seismicity corresponding to a crustal-scale fault (Fig. 6c,g). The long, narrow zone of low V_P is probably the boundary with a forearc block.

Additional synthetic tests have been carried out to confirm the resolving power of the major structures observed in the velocity tomogram. In our target resolution test, the synthetic velocity model utilized a 5% lower-velocity anomaly than the background (Fig. 7a–d). After inversion, the low-velocity anomaly was successfully recovered, although the amplitude of anomaly was slightly small (Fig. 7e–h).

Although the origin of the low-velocity zone remains unclear, it is very probably related to the complex history and evolution of the arc–continent collision. In the forearc region, sediments are mainly derived from the accretionary prism (Fig. 6a,e); as shortening increases with continued collision, sediments in the forearc become trapped between the plates (Eurasian and Philippine Sea), resulting in a zone of east-dipping back thrusts (Fig. 6b,f). The high-velocity anomaly imaged at about a 15-km depth in the east offshore area represents the submarine arc on the Philippine Sea plate. At this stage, soft materials at shallow depth (< 15 km) are still unable to accumulate sufficient tectonic energy, while lithified sediments at deeper depths (> 15 km) can. Along C–C′ (Fig. 6c,g), the Philippine Sea plate is completely accreted onto the Eurasian continent. Along a solid contact in the subsurface between the two plates, significant amounts of tectonic force are released by episodic earthquakes along the crustal-scale boundary.

Conclusions

Comparison of a 3D velocity model with reliable earthquake locations in the actively evolving plate collision zone of southeastern Taiwan highlights variations in subsurface structure resulting from the evolution of the ongoing collision process. High-quality earthquake data from numerous seismic stations have permitted construction of a reliable, detailed 3D *P*-wave velocity model for this young tectonically active area. Many features in this study on a 3D *P*-wave

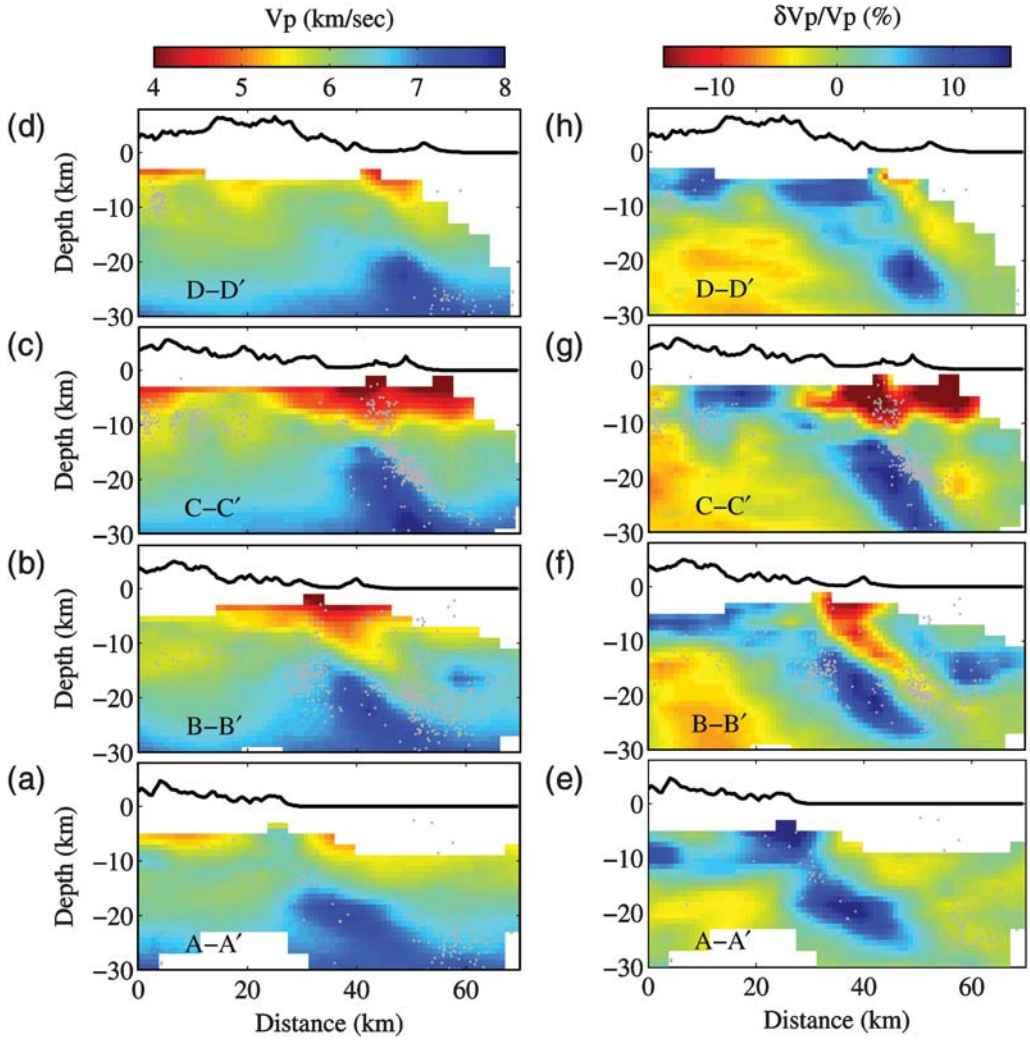

Figure 6. Sectional views of the velocity model and earthquake hypocenters. (a)–(d) Sectional views of the *P*-wave velocity model. (e)–(h) Sectional views showing percent perturbation of the *P*-wave velocity model. Earthquake hypocenters are presented as gray dots. For locations of the four profiles, see Figure 5a.

velocity model confirm previously known structural features in the study area (Kim *et al.*, 2005, 2006; Wu *et al.*, 2007; Cheng, 2009). However, a few previously unknown features have also been identified. The latter include an east-dipping low-velocity zone that separates higher-velocity anomalies to its east and west. This low-velocity zone narrows northward into an area of more advanced collision. The precise relocation of earthquake hypocenters using the new 3D velocity model also supports this observation. Collisions in eastern Taiwan are generally accepted to be more advanced in the north than the south, and therefore, the spatial variation in the width of the weak zone may be regarded as a temporal progression from an earlier to more advanced state of collision. Soft materials trapped along the crustal-scale weak zone compact as the Philippine Sea plate converges with the Eurasian plate. In the initial stage of collision, the soft, uncompacted sediment is not capable of accumulating tectonic forces. As compaction continues and the thickness of the zone of weakness diminishes, a significant amount of strain energy can be accommodated along the narrow crustal-scale weak zone, which is released by episodic seismic events. Northward-increasing seismicity along the proposed weak zone and northward narrowing of the zone of weakness indicate that the crustal-scale fault represents not only the interface between contrasting lithologic entities but also the progressive evolution of the tectonic state from early collision to advanced collision.

Data and Resources

Data in this study were collected by the Institute of Earth Sciences, Academia Sinica, Taiwan, University of Memphis, and Taiwan Central Weather Bureau. Data may be obtained from the corresponding parties upon request. Figure 1 was prepared using the Generic Mapping Tools (Wessel *et al.*, 1991).

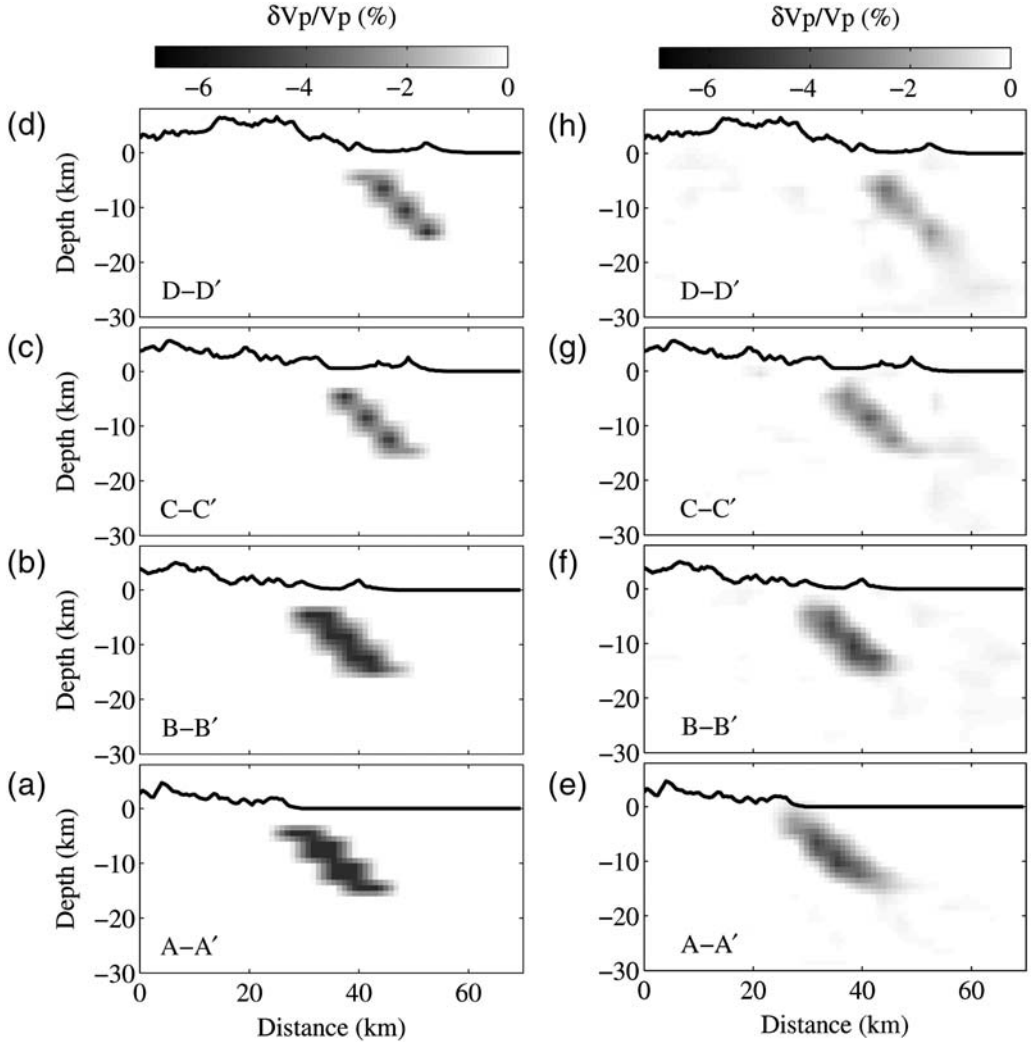

Figure 7. Synthetic test to evaluate the resolution of the low-velocity anomaly. Target structures are set up to imitate those recognized in tomographic sections. (a)–(d) are the input models and (e)–(f) are the results of inversion of synthetic data computed from input anomaly shown in (a)–(d).

Acknowledgments

The authors would like to express their appreciation for valuable comments and suggestions from two anonymous reviewers and Haijiang Zhang. This work was funded by the Korea Meteorological Administration Research Development Program under Grant CATER 2006–5101 and 2011–5310 (K. H. Kim). It was also sponsored by the National Science Council, Taiwan, under Grant NSC99-2116-M-001-021, through the Institute of Earth Sciences, Academia Sinica (K. C. Chen).

References

Benz, H. M., B. A. Chouet, P. B. Dawson, J. C. Lahr, R. A. Page, and J. A. Hole (1996). Three-dimensional *P* and *S* wave velocity structure of Redoubt Volcano, Alaska, *J. Geophys. Res.* **101,** 8111–8128.

Chai, B. H. T. (1972). Structure and tectonic evolution of Taiwan, *Am. J. Sci.* **272,** 389–422.

Chang, C. P., J. Angelier, C. Y. Huang, and C. S. Liu (2001). Structural evolution and significance of a mélange in a collision belt: The Lichi Mélange and the Taiwan arc-continent collision, *Geol. Mag.* **138,** 633–651.

Chen, K.-C. (1995). Earthquake studies using the PANDA and PANDAII seismic arrays, *Ph.D. Thesis, CERI/Dept. of Geological Science*, The University of Memphis, Memphis, Tennessee, 120 pp. .

Cheng, W. B. (2009). Tomographic imaging of the convergent zone in eastern Taiwan–A subducting forearc sliver revealed?, *Tectonophysics* **466,** no. 3–4, 170–183.

Chen, Y. L. (1995). Three-dimensional velocity structure and kinematic analysis in the Taiwan area, *Master's Thesis*, National Central University, Jhongli City, Taiwan, 172 pp.

Chen, H., J.-M. Chiu, J. Pujol, K.-H. Kim, K.-C. Chen, B.-S. Huang, Y.-H. Yeh, and S.-C. Chiu (2006). A simple algorithm for local earthquake location using 3D V_P and V_S models: Test examples in the central United States and in eastern Taiwan, *Bull. Seismol. Soc. Am.* **96,** 288–305.

Chiu, J.-M., S.-C. Chiu, and S. K. Kim (1997). The significance of the crustal velocity model in local earthquake locations from a case example of a PANDA experiment in the central United States, *Bull. Seismol. Soc. Am.* **87,** 1537–1552.

Eberhart-Phillips, D. (1986). Three-dimensional velocity structure in Northern California Coast Ranges from inversion of local earthquake arrival times, *Bull. Seismol. Soc. Am.* **76,** 1025–1052.

Ho, C. S. (1988). An Introduction to the Geology of Taiwan Explanatory Text of the Geologic Map of Taiwan, Central Geological Survey/ The Ministry of Economic Affairs, Taipei, Taiwan, 192 pp.

Huang, C.-Y., C.-W. Chien, B. Yao, and C.-P. Chang (2008). The Lichi Mélange: A collision mélange formation along early arcward back-thrusts during forearc basin closure, Taiwan arc-continent collision, *The Geological Society of America Special Paper* **436,** 127–154, doi 10.1130/2008.2436(06).

Huang, C.-Y., P. B. Yuan, S.-R. Song, C.-W. Lin, C. Wang, M.-T. Chen, C.-T. Shyu, and B. Karp (1995). Tectonics of short-lived intra-arc basins in the arc-continent collision terrane of the Coastal Range, eastern Taiwan, *Tectonics* **14,** 19–38.

Kim, K.-H., K.-C. Chen, J.-H. Wang, and J.-M. Chiu (2010). Seismogenic structures of the 1999 M_w 7.6 Chi-Chi, Taiwan, earthquake and its aftershocks, *Tectonophysics* **489,** 119–127.

Kim, K.-H., J.-M. Chiu, J. Pujol, K.-C. Chen, B.-S. Huang, Y.-H. Yeh, and P. Shen (2005). Three-dimensional V_P and V_S structural models associated with the active subduction and collision tectonics in the Taiwan region, *Geophys. J. Int.* **162,** 204–220.

Kim, K.-H., J.-M. Chiu, J. Pujol, and K.-C. Chen (2006). Polarity reversal of active plate boundary and elevated oceanic upper mantle beneath the collision structure in central eastern Taiwan, *Bull. Seismol. Soc. Am.* **96,** 796–806.

Liang, W.-T., J.-M. Chiu, and K.-H. Kim (2007). Anomalous *Pn* waves observed in eastern Taiwan: Implications of a thin crust and elevated oceanic upper mantle beneath the active collision-zone suture, *Bull. Seismol. Soc. Am.* **97,** 1370–1377, doi 10.1785/0120060226.

Lin, C.-H., Y.-H. Yeh, H.-Y. Yen, K.-C. Chen, B.-S. Huang, S. W. Roecker, and J.-M. Chiu (1998). Three-dimensional elastic wave velocity structure of the Hualien region of Taiwan: Evidence of active crustal exhumation, *Tectonics* **17,** 89–103.

Mandal, P., and J. Pujol (2006). Seismic imaging of the aftershock zone of the 2001 M_w 7.7 Bhuj earthquake, India, *Geophys. Res. Lett.* **33,** L05309, doi 10.1029/2005GL025275.

Podvin, P., and I. Lecomte (1991). Finite difference computation of traveltimes in very contrasted velocity models: A massively parallel approach and its associated tools, *Geophys. J. Int.* **105,** 271–284.

Shen, P. (1999). Simultaneous travel time inversion for 3D velocity model and earthquake locations: Application to the Northridge, California, 1994 mainshock–aftershock sequence, in *Geological Science*, University of Memphis, Memphis, Tennessee, 117 pp.

Snoke, A. J., and J. C. Lahr (2001). Locating earthquakes: At what distances can the Earth no longer be treated as flat?, *Seismol. Res. Lett.* **72,** 538–541.

Teng, L. S. (1990). Geotectonic evolution of late Cenozoic arc-continent collision in Taiwan, *Tectonophysics* **183,** 57–76.

Vidale, J. E. (1988). Finite-difference calculation of travel times, *Bull. Seismol. Soc. Am.* **78,** 2062–2076.

Wessel, P., and W. H. F. Smith (1991). Free software helps map and display data, *Eos Trans. AGU* **72,** 441, 445–446.

Wu, Y.-M., C.-H. Chang, L. Zhao, J. B. H. Shyu, Y.-G. Chen, K. Sieh, and J.-P. Avouac (2007). Seismic tomography of Taiwan: Improved constraints from a dense network of strong motion stations, *J. Geophys. Res.* **112,** B08312, doi 10.1029/2007JB004983.

Zhao, D., and H. Kanamori (1992). *P*-wave image of the crust and uppermost mantle in Southern California, *Geophys. Res. Lett.* **19,** 2329–2332.

Wu, Y.-M., Y.-G. Chen, C.-H. Chang, L.-H. Chung, T.-L. Teng, F. T. Wu, and C.-F. Wu (2006). Seismogenic structure in a tectonic suture zone: With new constraints from 2006 M_w 6.1 Taitung earthquake, *Geophys. Res. Lett.* **33,** L22305.

Korea Ocean Research and Development Institute
Ansan, Korea
kwanghee@kordi.re.kr
(K.-H.K.)

Institute of Earth Sciences
Academia Sinica
Taipei, Taiwan
chenkc@ies.earth.sinica.edu
(K.-C.C.)

Center for Earthquake Research and Information
University of Memphis
Memphis, Tennessee, USA
jerchiu@memphis.edu
(J.-M.C.)

National Central University
Jhongli, Taiwan
yenhy@earth.sinica.edu.tw
(H.-Y.Y.)

Manuscript received 22 January 2011